Dynamics of Hydrides on Hydrogen-Terminated Silicon (111)−(1×1) Surface

J. H. Ye,*,† T. H. Bok,‡ J. S. Pan,† Sam F. Y. Li,†,‡ and J. Y. Lin§

Institute of Materials Research and Engineering, Block S7, Level 3, Science Drive 4, National University of Singapore, 10 Kent Ridge Crescent, Singapore 119260, Department of Chemistry, National University of Singapore, 10 Kent Ridge Crescent, Singapore 119260, and Department of Physics, National University of Singapore, Lower Kent Ridge Road, Singapore 119260

Received: November 6, 1998; In Final Form: March 19, 1999

X-ray photoelectron spectroscopy (XPS) and static secondary ion mass spectrometer (SSIMS) have been applied to characterize Si(111) surface treated with 40% NH_4F solution. As-treated Si(111) surface is predominately terminated with monohydrides and free of contamination. The dynamics of etching process on ultra-clean atomically flat hydrogen-terminated Si(111) surface in 40% NH_4F solution has been examined at various potentials including the open circuit potential (OCP) by using in situ electrochemical scanning tunneling microscopy (ECSTM). Two distinct mechanisms are observed: (1) dihydride terminated step silicon atoms are dissolved much faster than the defect-free monohydride terminated ones; (2) dihydrides in the corner of {110} zigzag enclosed characteristic triangular pits lead to fast erosion of silicon atoms. Our results explain dynamic mechanics in formation of triangular pits on atomically flat silicon (111) surface in solution.

Introduction

The preparation of ultraclean silicon surfaces is a very important step in the manufacturing of semiconductor devices.[1] The silicon surface free of contaminants, impurities, roughness, and native oxide ensures the gate oxide integrity in a transistor. In wet cleaning of silicon surface, RCA standard cleaning process[2] is predominant in silicon very-large-scale integration (VLSI) technology because of its effective removal of particles, organics and metallic impurities from Si(001) surface. RCA wet chemistry, since its invention in 1960,[2] has been modified to meet the increasing demands of wafer processing as the dimensions of electronics devices are shrinking. It has been found that microroughening of silicon surface, which is caused by the continuous chemical growth and etching of hydrous oxide film on silicon in standard SC-1 solution, has an effect on the dielectric breakdown characteristics of gate oxide, particularly as the gate oxide is becoming thinner.[3,4] By varying the ratio of SC-1 cleaning composition from 1:1:5 to 0.05:1:5 (NH_4OH:H_2O_2:H_2O), the surface roughness can be reduced from 8 to 2 Å. However, alternative wet chemical cleaning technologies have been proposed such as HF- and sulfuric acid-based cleanings. An advanced wet cleaning process proposed omits conventional RCA SC-2 step when ozoned ultrapure water and highly purified HF solution are used.[5] A new cleaning concept developed at IMEC (Interuniversity Microelectronic Center) separates the oxidizing and the etching solutions; the IMEC cleaning consisting of H_2SO_4:H_2O_2 and HF/IPA has the highest yield among wet cleaning methods.[6] The challenges for wet chemistry are minimization of contamination, metallic impurities, and surface roughness as well as improvement of rinsing efficiency.[7]

Wet chemical etching of Si(111)[8−13] and Si(100)[14−17] has been extensively investigated by using ex situ scanning tunneling microscopy in the past few years. Pioneer work by Hessel et al.[8] and Higashi et al.[9] demonstrated that atomically flat Si(111) was prepared with 40% NH_4F vs atomically rough surface produced with 10% HF. Hessel et al.[8] reported for the first time the step flow etch mechanism where the dissolution of silicon occurred along the most stable $(1\bar{1}0)$ step with (111) microfacets. Sizes and shapes of the triangular pits in the topmost layer strongly depend on the pH of etching solutions. Recently, Houbertz et al.[12] have reported the potential-dependent etching of Si(111) in 40% NH_4F solution, in which the morphologies of Si(111) surfaces at anodic, OCP, and cathodic potentials were visualized. These experiments revealed pronounced effects of the sample potential on the anisotropy of etch process and etch rates by ex situ STM. Wade et al.[13] discovered that oxygen dissolved in 40% NH_4F solution initiated the formation of triangular etch pit on the terraces of Si(111) surface and peroxide ion radical reduced from oxygen resulted in abstraction of hydrogen which terminated silicon surfaces. The technically important Si(100) surface was studied with UHV-STM after wet chemical etching in 40% NH_4F, HF/HCl, and HF solutions.[14−17] Neuwald et al.[14] investigated wet chemical etching of Si(100) surface in 40% NH_4F solution. Etching of Si(100) in 40% NH_4F solution led to formation of small, (2×1)H dimer row reconstructed (100) terraces and pyramids with (111) facets of roughly constant sizes. A nearly ideal Si(100) surface was prepared by a wet chemical method with HF/HCl solution.[15,16] The surface was found to be covered by uniform dihydride phases as revealed by ex situ STM. The suppression of the (111) facet formation due to a low concentration of OH^- ions in the etchant solution and the stabilization of surface structure due to the formation of the ordered steps were proposed to be the main factors to produce such atomically flat Si(100) surface. More recently, Endo et al.[17] reported that ideally H-terminated Si(100) surface was prepared by using diluted HF solution and ultrapure water with very low dissolved oxygen and total organic carbon contents. It was suggested that ideally dihydride (1×1) surface should be formed by the preferential etching of every other row of the Si(100) surface.

* To whom correspondence should be addressed. E-mail: jh-ye@imre.org.sg.
† Institute of Materials Research and Engineering.
‡ Department of Chemistry.
§ Department of Physics.

10.1021/jp984341z CCC: $18.00
Published on Web 07/15/1999

Ex situ scanning tunneling microscopy results in information about the morphology and mechanics of silicon surface after wet chemical cleaning. However, ex situ techniques are not able to provide real time images to interpret the mechanics for etching process since the location would not be the same if the experimental parameters (e.g., the potential) are changed. Moreover, variations from wafer to wafer and site to site within wafer may lead to the different morphologies, which are not dependent of etching solutions. It is obvious that the pursuit of ultra-large-scale or nanometer-scale technology has necessitated the development of surface characterization methods that enable better understanding of the mechanism by an in situ monitoring of the wet etching process on an atomic scale. In situ electrochemical scanning tunneling microscopy (ECSTM) has been proved to be a powerful tool to characterize the microscopic details at solid/liquid interface on an atomic scale.[18] Atomic level understanding of silicon etching process[19] is extremely important for developing an alternative solution which is superior to the exclusively used RCA standard cleaning. Great attention has been paid to the solutions containing fluorine[8−22] and alkaline solution.[23−25] Although etching processes in various solutions have been studied for many years with STM[8−17] and other spectroscopic techniques such as FTIR,[26,27] direct observation of the etching process at the OCP that resembles the real wet chemical cleaning of silicon has not been reported yet.

We have used ex situ X-ray photoelectron spectroscopy (XPS)/static secondary ion spectrometer (SSIMS) and in situ electrochemical STM to characterize the Si(111) surface treated with 40% NH_4F solution and study potential dependence of etching process on Si(111) in 40% NH_4F solution.

Experimental Section

The sample with the area of 1×1 cm^2 was cut from Arsenic-doped *n*-Si(111) wafer with $(\bar{1}\bar{1}2)$ miscut less than 0.15° (Virginal Semiconductor, Inc.) and carefully boiled in nitric acid followed by cleaning with acetone, ethanol, and DI water (>18.2 MΩ) in an ultrasonic bath before each experiment. The sample was etched in 1% HF for 30 s followed by 40% NH_4F with pH of 7.3 for 3 min. The STM images were collected with typical constant tunneling current of 5 nA under cathodic potential control or at the OCP. A specially designed cell made of Teflon was used for in situ STM on a Nanoscope E system (Digital Instruments, Santa Barbara, CA). W tip was electrochemically etched in 1 N NaOH solution and coated with nail polish for in situ STM experiment. Platinum wires were used as counter and reference electrodes. All the potentials in this work are quoted vs the standard calomel electrode (SCE). Teflon wares were employed for the cleaning step to avoid or minimize any contamination. Ammonium fluoride NH_4F (VLSI grade) was used as received.

XPS was performed with VG ESCALAB-220iXL with a monochromator Al Kα radiation beam (1486.6 eV) with a UHV chamber better than 10^{-10} Torr. All binding energies in XPS spectra were calibrated against the neutral C_{1s} peak at 284.6 eV to compensate for the surface charging effect. SSIMS was carried out with VG ESCA MKII XPS system with SIMS spectrometer. Argon primary beam with 1 nA and 2 keV was used in all SSIMS experiments.

Results and Discussion

X-ray photoelectron spectroscopy (XPS) was used to characterize the surface states of silicon (111) treated with 40% NH_4F solution. A wide-range spectrum shows the typical features of silicon 2p and 2s peaks with the 2p peak located at

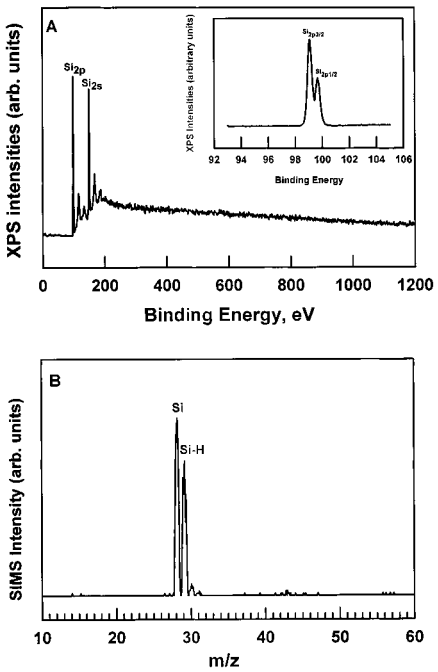

Figure 1. (A) X-ray photoelectron spectroscopy and (B) static secondary ion mass spectrometry (B) of hydrogen-terminated Si(111) surface. The surface was treated with 1% HF for 30 s and 40% NH_4F (pH = 7.3) for 3 min without DI water rinse. The difference in binding energy between $Si_{2p3/2}$ and $Si_{2p3/2}$ is 0.6 eV, and the ratio of $Si_{2p3/2}$ and $Si_{2p3/2}$ peaks is about 0.5.

99.0 eV (Figure 1A). Narrow range integrated scan revealed that no silicon oxide was formed and only very trace level of carbon was present, which was adsorbed during the transferring process from air to UHV chamber. Silicon $2p_{3/2}$ and $2p_{1/2}$ peaks were distinguishable with Al monochromator (1486.6 eV) of resolution of 0.4 eV (Figure 1A, inset). The XPS results indicate that the as-treated surface was free of contamination of carbon and oxide (Figure 1A and the inset). Secondary ion mass spectrometer (SSIMS) was employed to examine the surface termination. Figure 1B shows that the as-treated Si(111) surface gives very strong intensities at the mass/charge (*m*/*z*) of 28 and 29 and weak responses at 30 and 31. The SIMS signal responses (abundance) for pure silicon isotopes are 92.23%, 4.67%, and 3.10% for the masses 28, 29, and 30. The strong response at *m*/*z* of 29 is assigned to monohydride-terminated silicon. The strong Si−H peak suggests the silicon surface is predominately terminated with one hydrogen. The SSIMS results are consistent with those revealed by attenuated total reflection fourier transmission infrared (ATR−FTIR).[26,27] In SSIMS spectrum, silicon mass 28 shows a very strong peak followed by Si−H. The dihydrides and trihydrides are not quantitatively distinguishable from SSIMS results. Apparently, dihydrides and trihydrides as well as oxide were not present on the silicon surface, which differs from the surface, treated with NaOH.[28] Negative SSIMS results show the silicon surface treated in the NH_4F for 3 min without DI water rinse has strong intensities at the *m*/*z* of 16 and 19 that are O^- and F^-, respectively. F^- signal indicates that fluoride dissociated from NH_4F adsorbed on some regime of the silicon surface rather than the products from the etching reaction because no SiF_4^- was detected in the negative SSIMS. The results from XPS and SSIMS suggest that the H-terminated silicon surface prepared with 40% NH_4F have predominately monohydride-terminated surface with a very trace amount of fluoride adsorption.

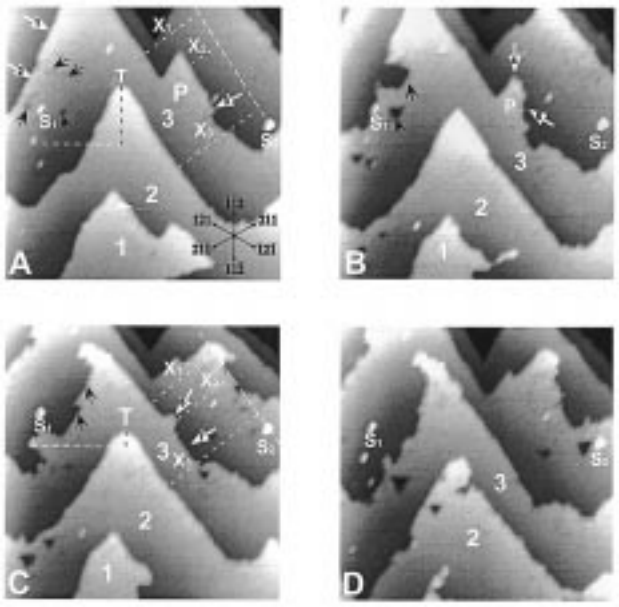

Figure 2. Real time STM images of H-terminated Si(111) surface at the open circuit potential in the neutral NH_4F solution. The potential of Si(111) is -1.09 ± 0.01 V vs SCE, which is 10 mV more negative than the open circuit potential (OCP) of -1.08 V. $I_{tunneling} = 5$ nA, $E_{tip} = -570$ mV. Acquisition rate, 30 s per frame; image area, 500 nm by 500 nm. The time interval between two consecutive frames is 30 s. S_1 and S_2 are used to mark the bright spots as indicators for the thermal drift.

We applied the potential of -1.09 V to silicon substrate, which was practically the same as the open circuit potential (OCP) of -1.08 V. If the potential was set to the OCP, small grains randomly distributed over atomically flat Si(111) surface, which was similar to those observed in wet etching of silicon previously.[8] Allongue et al.[23] suggested that the dissolution of silicon atoms was controlled by chemical reaction taking place at Si/electrolyte interface at the OCP. At -1.09 V, electrochemical reaction was minimized and the oxidation was avoided by maintaining the potential to -10 mV apart from the OCP. An STM image (500 nm $\times$ 500 nm) of an H-terminated Si(111)$-(1\times1)$ (Figure 2A) shows saw-tooth shaped terraces of H-terminated silicon surface with typical terrace width of 200 nm. Hessel et al.[8] also reported similar saw teeth shape of Si(111) surface in an ex situ STM experiment. The saw-tooth shaped terrace was proposed to result from (100) facets at step edge with two dangling bond exposed to etching solution.[29] However, in situ observation of the step-flow etching process has not been observed and the mechanism for forming triangular pits as well as saw tooth terraces has not been elucidated. In the present work, real time STM images of etching process on H-terminated Si(111) surface were recorded in 40% NH_4F solution near the OCP (shown in Figure 2). The orientation on Si(111) is indicated on the right corner of the images. Two bright spots marked with S_1 and S_2 are used to label the thermal drift during the experiment and calibrate etch rate estimation. In the estimation of etch rate, the etch rate and surface morphology were evaluated from 9 points across 3 in. wafers. Typically, the variations of etch rate are within 10% and the terraces at edge are smaller than in the center. The representative morphologies in the wafer center were presented. In Figure 2A, the steps marked with arrows 1 and 2 are straight outward $(1\bar{2}1)$. The step consists of (101) atom chains forming an angle of $\theta = 35.26°$ with a (111) plane according to $\theta = \cos^{-1}[(h_1h_2+k_1k_2+l_1l_2)/\sqrt{(h_1^2+k_1^2+l_1^2)(h_2^2+k_2^2+l_2^2)}]$, where (h_1,k_1,l_1) and (h_2,k_2,l_2) represent Miller indexes for the two planes forming the angle. Note that the direction of the (101) atom chains are not the same as the $(1\bar{1}0)$ direction mentioned in the previous paper[8] where the $(1\bar{1}0)$ is outward normal to $(11\bar{2})$ or the (111) plane. We found that the region denoted by arrow 2 was eroded faster than that by arrow 1. On layer 3 in Figure 2A and C, the step in the direction of $(1\bar{2}1)$ retracted at a maximum etch rate of 105 nm/min in the region where the small triangle exists (Figure 2B, in black arrow). Ideal monohydride-terminated silicon step oriented in $(1\bar{2}1)$ as denoted by arrow 2 has a lower etch rate. The faster etch rate is attributed to the irregular defect pits on the (111) plane (in black arrows, Figure 2A) instead of kink sites. A kink site containing a monohydride-terminated step existed in the region marked with P in Figure 2A. The kink site indicated by arrow 3 rendered fast dissolution of silicon atoms in the $(\bar{2}11)$ direction. Kink sites-induced etching was developed into a region where there were two step edges terminated by dihydrides as indicated by arrows 4 and 5 in Figure 2B. These dihydrides facilitate the dissolution of silicon atoms in two directions along $(\bar{1}\bar{1}2)$ and $(\bar{1}2\bar{1})$. We found that the faster etch rate of silicon atoms induced by dihydrides was faded at monohydride terminated silicon steps as denoted by arrows 6 and 7 in the $(\bar{2}11)$ direction shown in Figure 2C, which were terminated by monohydrides. For example, the retraction of the terrace X_2 was much faster than the step X_1. From the etching rates of 63 nm/min at the step X_2 and 21 nm/min at the step X_1 and X_3, we infer that faster etch rate at step X_2 is induced by dihydrides-terminated steps in the direction of $(\bar{1}\bar{1}2)$ and $(\bar{1}2\bar{1})$ in which the dihydrides are developed from the kink sites as denoted by arrow 3 (Figure 2A). The dihydrides facilitate the dissolution of silicon atoms until it reaches the monohydride-terminated terrace in the $(\bar{2}11)$ direction (X_1 and X_2 in Figure 2C). This phenomenon clearly shows that the monohydride-terminated step is more stable than the dihydrides and kink site contained monohydride steps. This was also reported in the previous paper.[20] It is obvious that there are differences between the two. First at all, the applied potential (-10 mV negative than the OCP) was different from that by Kaji et al.[20] where more cathodic potential was employed; the second, the solution used in the present work (40%) was also different from that (1% NH_4F);[20] the third, etching of silicon was of step-flow mechanism, i.e., all terraces exposed to solution were etched away along defined directions while the terrace dissolution in 1% NH_4F was of layer by layer fashion, i.e., the top layer was first dissolved followed by the second layer. These differences possibly resulted from the compositions of etching solutions used. On layer 2, there are no kink sites and defects existing on the surface shown in Figure 2A. Both terrace steps are terminated with monohydride with (101) and (011) chains in the $(1\bar{2}1)$ and $(\bar{2}11)$ directions, respectively. The step toward $(\bar{2}11)$ dissolved at 28 nm/min as estimated from the retraction from the terrace X_3. The value is the same as on the portion X_1 of the terrace on layer 3. On the triangular tip marked with T (Figure 2A), the dihydrides are the exclusive terminated species which are outward $(\bar{1}\bar{1}2)$ with two peripheries oriented outward $(1\bar{2}1)$ and terminated with the monohydrides. From Figure 2A and C, the retraction of the dihydride-terminated tip T (86 nm/min) is 3 times as fast as those steps terminated with monohydrides in the $(1\bar{2}1)$ and $(\bar{2}11)$ directions (28 nm/min). The values characterize the real etching rate of pure dihydrides and monohydrides.

After we changed the potential to -1.13 V which was 50 mV more negative than the OCP, the Faradaic current was about -1 to 3 $\mu A/cm^2$ and in situ imaging of the formation of

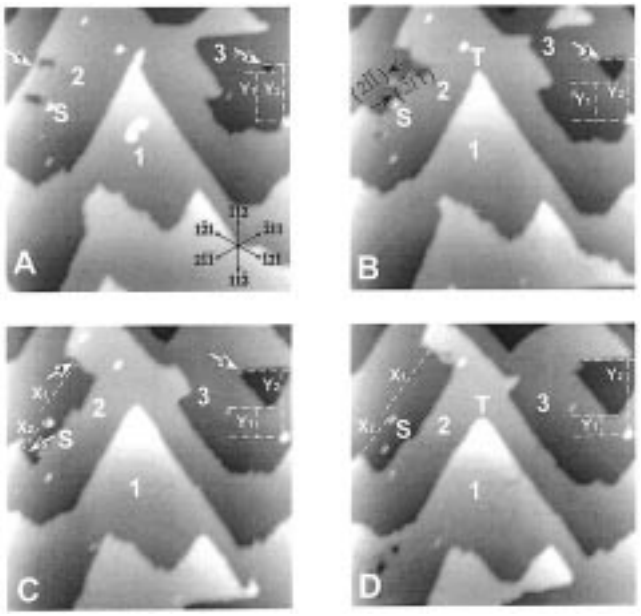

Figure 3. Real time STM images of H-terminated Si(111) surface in the neutral NH_4F solution. The potential of Si(111) is -1.13 ± 0.01 V vs SCE, which is 50 mV more negative than the open circuit potential (OCP) of -1.08 V. $I_{tunneling} = 5$ nA; $E_{tip} = -570$ mV. Acquisition rate, 30 s per frame; image area, 500 nm by 500 nm. The time interval between two consecutive frames is 60 s. S_1 and S_2 are used to mark the bright spots as indicators for the thermal drift.

triangular pits was performed (Figure 3). As we know, the mechanism for formation of triangular pits has been of great scientific and technological significance. However, so far no clear images show real formation mechanism for triangular pits under potential control in an in situ STM experiment. Allongue et al.[23,25] evaluated growth of triangular pits in alkaline solution at extremely cathodic potential with current of -200 $\mu A/cm^2$. In the region of weak hydrogen evolution (-40 $\mu A/cm^2$), irregular pits appeared.[25] In this work, the solution used (40% NH_4F) etches silicon at an etch rate much slower than alkaline solution. Faradaic current of -1 to 3 $\mu A/cm^2$ indicated that a slight electrochemical reaction took place.[23] The STM images of the same scan direction were collected via selecting every other scan within a time interval of 1 minute. The formation of irregular pits (arrow 1) and regular triangular one (arrow 2) occurred on layers 2 and 3, respectively (Figure 3A). The straight step of the terrace 2 outwards $(1\bar{2}1)$ was rather stable against the etching while the pits gradually grew. As the pits grew, the two kinds of steps formed (Figure 3B) in the $(\bar{1}\bar{1}2)$ and $(\bar{2}11)$ directions in which the steps were terminated by jagged dihydrides and monohydrides, respectively. It was observed that the step marked with arrow 4 retracted in the direction $2\bar{1}\bar{1}$) faster than that in the direction $(\bar{2}11)$ (Figure 3C and D) as revealed by the extension of X_1 and X_2. The dihydride-terminated step as indicated by arrow 4 was dissolved at 28 nm/min, which was 4 times faster than the 7 nm/min rate of the monohydride-terminated step as indicated by arrow 5. The ratio of etch rates (dihydride vs monohydride) is 4:1 compared with that (3:1) at the OCP. This is due to the jagged $(2\bar{1}\bar{1})$ dihydride-terminated steps. The other difference is that in situ monitoring of triangular pit formation was discernable at -1.13 V, but it was not observable at the OCP because of too fast etching rate. The real time STM images of the triangular pit formation were obtained as shown in Figure 3. At the beginning of the growth, the pit was small (arrow 2) but visible (Figure 3A). As time passed, the triangular pit grew into a much bigger pit (arrow 3, Figure 3B) and finally the pit was extended

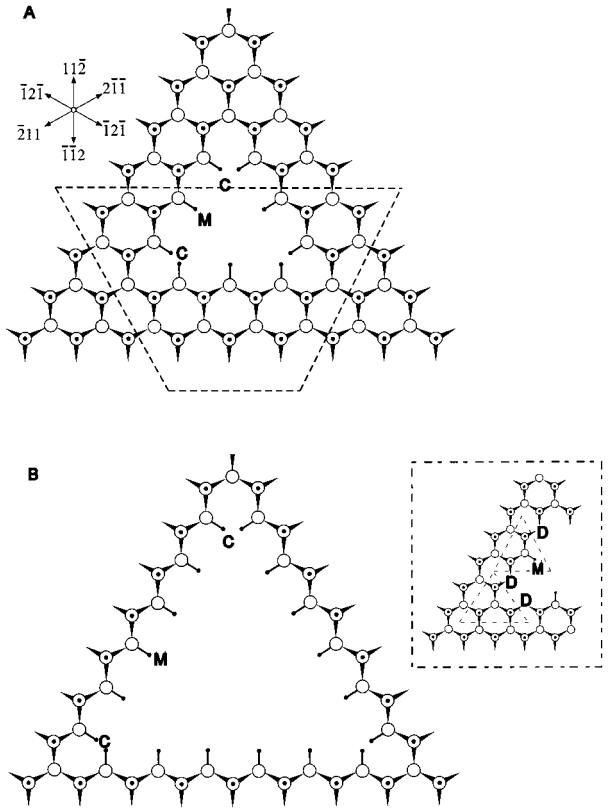

Figure 4. Ball-and-stick model of Si(111)-1×1:H surface prepared with 40% NH_4F (pH = 7.3) solution. The monohydrides on Si(111) and the bulk silicon atoms bonded to the monohydrides are shown as dot−circles and open circles. Sticks with a small fill circle represent hydrogen atoms. The arrows are used for the bond between the monohydride-terminated silicon and bulk silicon atoms.

(Figure 3C) until one of its enclosed peripheral was discontinued (Figure 3D). Etch rate for the growth of triangular pits was estimated in two directions $(11\bar{2})$ and $(\bar{1}\bar{1}2)$ via measuring the changes of Y_1 and Y_2. The variation of Y_1 was slightly larger than that of Y_2 as shown in Figure 3B and C. The ratio of the etch rate for the dihydrides and monohydrides $(\bar{1}\bar{1}2)$ and $(11\bar{2})$ was about 1:1. Note that the images and etch rates are the representatives from several independent experiments and samples. Width of terraces and etch rates vary within 10% experimental errors, depending on cutting samples.

Figure 4 shows a ball-and-stick model for the mechanism for the etching process occurring on the H-terminated Si(111) in the NH_4F. The region enclosed by the dashed line (Figure 4A) illustrates that the regime of T in the $(\bar{1}\bar{1}2)$ direction in layer 2 of Figure 2A, where the etch rate was much faster than the steps terminated with monohydrides in the $(\bar{2}11)$ and $(1\bar{2}1)$, is terminated by a row of dihydrides. The monohydride-terminated {110} zigzag chains always remain at lower potential than that of the dihydrides, so that the straight steps appear over atomically flat surfaces. The triangular pit was formed preferentially on the atomically flat terrace pointing to $(11\bar{2})$ (Figure 3). Three sides of the triangular pit consist of {110} chains, which have an angle of 35.26° with (111) surface. It was claimed that the triangular holes (pits) were comprised of (111)-type steps.[8] From the model we propose in this work (Figure 4), it is proper to state that the edges enclosing triangular pits are (110) type in order to better explain the difference in etching rate observed experimentally. Zigzag patterns are comprised of two (110)-type step and (100)-type tip. In this case, the difference in etching rate can be explained by the stability of

(111) and (110) steps. Apparently, the {110} is stable enough since there are no dihydrides that terminate both ends of the {110} chains. We think that steric effect plays an important role in the etching process on the Si(111) surface. As illustrated in Figure 4A, the smallest triangular pit has three sides, each consisting of {110} chains. The {110} chain has one center monohydride (M) and two-corner monohydrides (C) in which two corner monohydrides have strong steric interaction with their neighboring corner monohydrides on the other sides. The corner monohydrides are converted into dihydrides by losing two hydrogen atoms to form hydrogen. As the dihydrides are formed, the sides are not stable as they are before the formation of the dihydrides (D) as shown in the inset of Figure 4B. The ends of each side are terminated with two dihydrides (D), which are obviously etched away much faster that the monohydrides in the center of the {110} chains. These dihydrides initiate and facilitate the etching along the {110} chains like the case in Si(110) surface.[19] The etching process removes the regime enclosed by two dash triangles (Figure 4B, inset) and a big triangle is formed as shown in Figure 4B. The corner monohydrides are present at the tips of triangular shapes. The etching process is continuously initiated by the presence of the corner monohydrides (C in Figure 4B). We refer the corner monohydride as metastable monohydride present on the H-terminated Si(111) surface. The etch rates in the $(11\bar{2})$ and $(\bar{1}\bar{1}2)$ directions are almost the same (35 nm/s), suggesting that {110} chains perpendicular to $(11\bar{2})$ which is terminated with monohydride be dissolved from the both ends of the {110} chain. Since we have observed straight sides of triangular pits, we conclude that the steps and the corners of triangular pits are always terminated with monohydrides and metastable monohydrides, respectively.

Energetic diagrams are considered as the Si(111) is immersed into the aqueous solution. Potential dependence on etching rate has been observed (Figure 2 and 3). Under these conditions, the bands are bent and positive charges are accumulated at the interfaces between the solid silicon and solution. The solution containing OH^-, H^+, F^-, NH_4^+, and OH^- is known to attack the silicon first to form Si−OH, which is further converted into SiF_4^- in the solution.[23−25] This is typical of chemical reaction occurring at the OCP[23] where the net flow current is zero and the etching rate reaches the highest value without formation of silicon oxide (Figure 5A). As the potential is set to 50 mV more negative than the OCP, the interface becomes partially negatively charged and hydrogen evolution starts to take place (Figure 5B). In this case, the OH^-, the only etching reagent, accesses less reactive sites at the silicon surface because the negative charges are distributed at the solid/liquid interface. Therefore, the etching rate is slowed down via giving up reactive sites for the hydrogen evolution reaction. Chemical ($OH^- + Si \rightarrow SiOH^-$) and electrochemical reactions ($H^+ + e \rightarrow H_2$) take place simultaneously. If the potential is further polarized negatively, the interface is occupied by negative charges and OH^- from aqueous side is repelled from the surface. In this case hydrogen evolution predominantly controls the total reaction and chemical reaction is stopped because no surface reaction sites are available for OH^- attack (Figure 5C).

Summary

In conclusion, we have characterized the Si(111) surface treated with NH_4F solution and studied the etching process of Si(111) in 40% NH_4F solution by XPS and SSIMS at the open circuit potential and under cathodic potential control by in situ scanning tunneling microscope. Si(111) surface is free of contamination and perfectly terminated with monohydrides as revealed by XPS and SIMS. High-resolution STM images of structural change in the etching process of hydrogen-terminated Si(111) suggest that dihydride and metastable monohydride should be induced sites for the etching process, and surface states (e.g., kink sites and pits) also act as trapping sites to start the dissolution of Si atoms. It is remarkable that formation of triangular pits has been monitored in situ and explained by theoretical model.

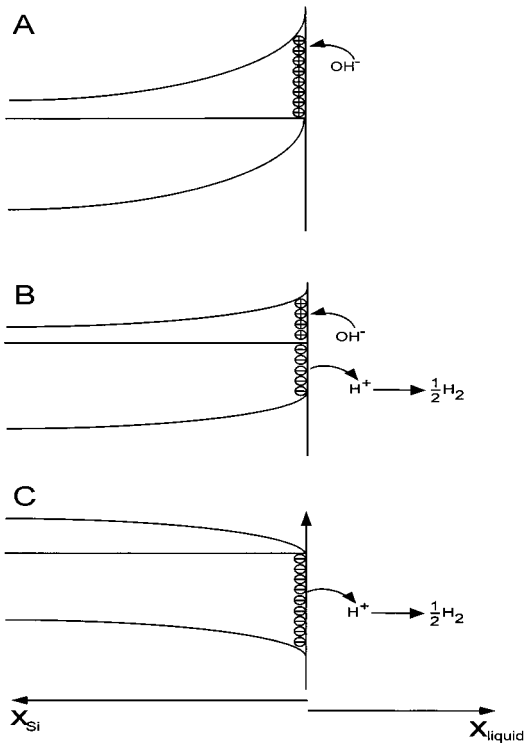

Figure 5. Schematic diagrams for the energetic level at the solid/liquid interface as silicon surface is in contact with a solution. (a) The interface was positive charges distributed at the OCP; (2) the interface is partially positively charged and negative charges reduce reactive sites for OH^- attack from solution; (c) the interface is predominately covered with negative charges where the OH^- attack is prohibited and hydrogen evolution takes place.

Acknowledgment. Financially support from National Science and Technology Board is gratefully acknowledged.

References and Notes

(1) *Handbook of Semiconductor Wafer Cleaning Technology: Science, Technology and Applications*, Kern W. Ed.; Noyes Publications: Park Ridge, New Jersey, 1993.
(2) Kern, W.; Pauotein, D. A. *RCA Rev.* **1970**, *31*, 187.
(3) Miyashita, M.; Tsuga, T.; Makihara, K.; Ohmi, T. *J. Electrochem. Soc.* **1992**, *139*, 526.
(4) Ohmi, T.; et al. *IEICE Trans. Electron.* **1992**, *7*, 800.
(5) Ohmi, T. *Proc.−Electrochem. Soc. Meeting* **1993**, *184*, p 495.
(6) Meyer, M. M.; et al. *Mat. Res. Soc., Symp. Proc.* **1993**, *315*, 35.
(7) Kern, W. *J. Electrochem. Soc.* **1990**, *137*, 1887.
(8) Hessel, H. E.; Feltz, A.; Reiter, M.; Memmert, U.; Behm, R. J. *Chem. Phys. Lett.* **1991**, *186*, 275.
(9) Higashi, G. S.; Becker, R. S.; Chabal, Y. J.; Becker, A. J. *Appl. Phys. Lett.* **1991**, *58*, 1656.
(10) Houbertz, R.; Memmert, U.; Behm R. J. *Appl. Phys. Lett.* **1993**, *62*, 2516.
(11) Houbertz, R.; Memmert, U.; Behm R. J. *J. Vac. Sci. Technol.* **1994**, *B12*, 3145.
(12) Houbertz R.; Memmert, U.; Behm R. J. *Surf. Sci.* **1998**, *396*, 198.
(13) Wade, C. P.; Chidsey, C. E. D. *Appl. Phys. Lett.* **1997**, *71*, 1679.
(14) Neuwald, U.; Hessel, H. E.; Feltz, A.; M.; Memmert, U.; Behm, R. J. *Surf. Sci.* **1993**, *296*, L8.
(15) Morita, Y.; Tokumoto, H. *Appl. Phys. Lett.* **1995**, *67*, 2654.
(16) Morita, Y.; Tokumoto, H. *J. Vac. Sci. Technol.* **1996**, *A14*, 854.

(17) Endo, K.; Arima, K.; Kataoka, T.; Oshikane, Y.; Inoue, H.; Mori, Y. *Appl. Phys. Lett.* **1998**, *73*, 1853.
(18) Itaya, K.; Sugawara, R.; Morita, Y.; Tokumoto, T. *Appl. Phys. Lett.* **1990**, *60*, 2534.
(19) Ye, J. H.; Kaji, K.; Itaya, K. *J. Electrochem. Soc.* **1996**, *143*, 4013.
(20) Kaji, K.; Yau, S. L.; Itaya, K. *J. Appl. Phys.* **1995**, *78*, 5727.
(21) Yau, S. L.; Kaji, K.; Itaya, K. *Appl. Phys. Lett.* **1995**, *66*, 766
(22) Allonque, P.; Keiling, V.; Gerischer, H. *Electrochim. Acta* **1995**, *40*, 1353.
(23) Allonque, P.; Keiling, V.; Gerischer, H. *J. Electrochem. Soc.* **1993**, *140*, 1009, and 1018.
(24) Allonque, P.; Keiling, V.; Gerischer, H. *J. Phys. Chem.* **1995**, *199*, 9472.
(25) Allonque, P.; Brune, H.; Gerischer, H. *Surf. Sci.* **1992**, *275*, 414.
(26) Higashi, G. S.; Becker, R. S.; Chabal, Y. J.; Becker, A. J. *Appl. Phys. Lett.* **1991**, *58*, 1656.
(27) Higashi, G. S.; Chabal, Y. J.; Trucks, G. W., Raghavachari, K. *Appl. Phys. Lett.* **1990**, *56*, 656.
(28) Allongue, P. *Phys. Rev. Lett.* **1996**, *77*, 1986.
(29) Olshanetzky, B. Z.; Repinsky, S. M.; Shklayae, A. A. *Surf. Sci.* **1977**, *69*, 205.